Adsorption of phenanthrene from aqueous solutions by biochar derived from an ammoniation-hydrothermal method

Xiaoqing Wang [a], Zizhang Guo [a], Zhen Hu [a], HuuHao Ngo [b], Shuang Liang [a], Jian Zhang [a,c,*]

[a] *Shandong Key Laboratory of Water Pollution Control and Resource Reuse, School of Environmental Science & Engineering, Shandong University, Qingdao 266237, P.R.China*

[b] *Centre for Technology in Water and Wastewater, School of Civil and Environmental Engineering, University of Technology Sydney, Ultimo, NSW, 2007, Australia*

[c] *State Key Laboratory of Microbial Technology, Shandong University, Jinan 250100, P.R.China*

[*] Corresponding author. Tel.: +86 0531 88369518; fax: +86 0531 88369518. *E-mail address*: zhangjian00@sdu.edu.cn.

Abstract

An innovative ammoniation-hydrothermal method of biochar production was developed for the adsorption of phenanthrene (PHE) from aqueous solutions in this paper. *Phragmites australis* (PA) was used to produce biochar in a hydrothermal kettle at 280℃ in muffle furnace using urea as an ammoniation reagent. Characterizations were executed by scanning electron microscope (SEM), N_2 adsorption/desorption isotherms, X-ray diffraction (XRD), elemental analysis, X-ray photoelectron spectroscopy (XPS) and Fourier transform infrared spectroscopy (FT-IR) to explore its morphological, physical, and chemical properties. Batch experiments of PHE adsorption were carried out to study the adsorption isotherms and kinetics. Quantum chemistry computational simulations were employed based on density functional theory (DFT) to establish and optimize adsorption configurations and analyze the biochar's structural effects on adsorption performance. Results showed that the ammoniation-hydrothermal method produced biochar with a higher surface area and a maximum equilibrium adsorption capacity of 1.97 mg/g. The adsorption fitted well with Freundlich isotherm model (R^2 > 0.96) and Pseudo-second-order kinetic model (R^2 > 0.82). Adsorption energy calculation revealed that the N functionalities, especially pyridine N in the N-doped biochar structure, exhibited stronger binding ability with PHE, which contributed most to the favorable adsorption ability of the ammoniation-hydrothermal biochar.

Keywords: Biochar; Ammoniation-hydrothermal method; Phenanthrene; Adsorption; Density functional theory

1. Introduction

Polycyclic aromatic hydrocarbons (PAHs) usually refer to a broad category of harmful and toxic contaminants in the ecosystem (Pang et al., 2019). They are produced when hydrocarbons or other organic compounds (such as coal, oil, and biomass) are incompletely burned (Kaya et al., 2013). Because PAHs are continuously released into the environment with their persistent nature, they compose an essential class of persistent organic pollutants (Gupta and Singh, 2018). Phenanthrene (PHE) is categorized with low molecular weight. However, it resembles high molecular weight PAH and has a medium solubility compared with other PAHs (Gupta, 2016); thus, it is selected as a representative for adsorption studies (Gupta and Singh, 2018). In the

past decades, researchers reported various methods for PAHs remediation from aqueous solutions. Despite the usability of techniques such as photo-catalyst degradation (Lee and Park, 2013) and bio-remediation (Chang et al., 2003), adsorption is the most applicable and widely used for PAHs removal from aqueous systems (Mittal et al., 2013; Khan et al., 2017).

Among all kinds of adsorbents, biochar is characterized by large surface area, developed porosity, and widely available raw materials. Therefore, it is regarded as a promising adsorbent for a wide range of water contaminants (Ge et al., 2016a; Huang et al., 2019) and has attracted full attention in the field of wastewater treatment. Moon and Shim (2006) proved that biochar derived from soybean stalk had better performance in PAHs adsorption compared with commercial activated carbon (AC). It has been reported that agricultural wastes-based biochar has favorable adsorption ability for naphthalene, phenanthrene, and pyrene (Yakout et al., 2013). Nevertheless, for an enhanced adsorption efficiency, especially the adsorption affinity to specific contaminants, it is significant to modify the biochar to adjust its physicochemical properties (Ge et al., 2016a). Gupta et al. (2014) reported that AC with higher surface basicity had greater adsorption affinity to contaminants in solutions. Based on this, their further study (Ge et al., 2016b) produced ammoniation-modified biochar under the microwave. The biochar obtained higher surface area, less oxygen-containing functional groups, and higher basicity, contributing to a high adsorption ability for pyrene. Our previous research (Guo et al., 2017) reported an activation method using ammoniation reagents for intensified pre-treatment of AC production, which significantly increased the adsorption ability of iodine by 20%. The ammonification loosened the lignocellulose structure of the raw material. Sequentially, the biochar was modified with enhanced surface area, porosity, and more functional groups on the surface (Givens et al., 1988; Guo et al., 2017).

However, the ammonification is usually achieved by a long period of immersion under a stable temperature (usually 25℃) (Guo et al., 2017), followed by pyrolysis at a high temperature ranging from 300 to 900℃in the absence of oxygen (Zhang et al., 2019), which increases the difficulty and time for biochar production. By comparison, hydrothermal carbonization (HTC), which refers to the synthesis of carbon-rich products using water as reaction medium in a sealed kettle (Mumme et al., 2011), requires lower reaction temperature (180-280℃) under self-pressure. It avoids the influence of water content in raw materials and has less energy consumption and CO_2

release at the same time (Benavente et al., 2015). Moreover, the increased number of functional groups on the biochar surface is a significant difference between HTC materials and other carbon materials (Gao et al., 2013). HTC has become an efficient method for preparing biochar with favorable properties (Reza et al., 2014). However, mixing ammoniation reagent with water in the HTC process to produce biochar is rarely reported, which could obtain ammoniation-modified biochar under low temperature in one step.

In this study, ammoniation-hydrothermal biochar was developed to explore its adsorption ability for PHE in aqueous solutions. On this basis, this study (i) evaluated the impacts of HTC treatment on biochar properties; (ii) investigated the effects of incorporated N functionalities on the biochar surface caused by ammoniation reagent; (iii) explored the adsorption configurations based on density functional theory (DFT) and the quantitative calculation of PHE adsorption ability on the biochar surface.

2. Materials and methods

2.1. Materials and chemicals

Phragmites australis (PA) is a very common aquatic macrophyte in China, and a great deal of withered PA is produced as solid waste every year. Withered PA is a rich source of lignocellulose, and biochar prepared from PA has been reported to have effective adsorption ability for several contaminants in aqueous matrices (Zhang et al., 2017; Wang et al., 2018; Wang et al., 2019). In this study, PA straws for biochar production were obtained from Baiyun Lake in Shandong Province. After cleaning and drying, the straws were mechanically shattered and ground into powder with the particle size < 1.0 mm. PHE solid used for adsorption experiments was of 95% purity, purchased from Aladdin Industrial Corporation. PHE-d_{10} standard (1000 mg/L, dissolved in CH_2Cl_2) and Custom Semivolatile Mix of 2-Fluorobiphenyl and P-Terphenyl-d_{14} (2000 mg/L, dissolved in acetone-hexane 1∶ 1) used for the preparation of GC-MS samples were purchased from o2si smart solutions (made in the USA). NaCl, CH_2Cl_2, urea, and methanol were of analytical grade. Besides, all solutions were prepared with distilled water.

2.2. Preparation of biochars

The ammoniation-hydrothermal biochar was produced using 10 g air-dried PA powder mixed with 1 g urea in 150 mL distilled water. The mixture was put in a hydrothermal kettle and heated up to 280℃ in a muffle furnace. After naturally cooling to the room temperature, the carbonized material was washed three times with

distilled water to remove the impurities and dried at 105℃ for 12 h, referred to as HABC. The biochar referred to HMBC was produced using 10 g PA powder in 150 mL distilled water without ammoniation reagent. For control, the following steps were consistent with the preparation method for HABC. The ammoniation-pyrolyzed biochar, referred to PABC, was prepared using 10 g dried PA powder mixed with a water solution containing 1 g urea in an incubator. After immersing under vacuum at 25℃ for 10 d, the mixture was put in a crucible and heated to 500℃ in a muffle furnace. High purity N_2 was flowed into the furnace to provide an oxygen-limited condition throughout the pyrolysis process. All other conditions and steps were the same as the other two biochars.

2.3. Characterization of biochars

The specific surface area, total pore volume, and pore size distributions of biochars were determined by N_2 adsorption/desorption isotherms using the surface area analyzer (Quantachrome Instruments, version 3.01) at 77 K after outgassing at 105℃ for 12 h. Surface topography of biochars was observed by a scanning electron microscopy (SEM, SEU8010). Contents of C, H, O and N in biochars were obtained by an Organic Elemental Analyzer (Vario EL III, USA). The crystallinity of biochars was investigated by the X-ray diffraction (XRD, Ultima IV) within the scanning range of 10 to 80° at a scanning speed of 10°/min. The surface chemical properties of biochars were tested by X-ray photoelectron spectroscopy (XPS, Thermo ESCALAB XI+). Fourier transform infrared spectroscopy (FT-IR) was analyzed for different types of functional groups on the biochar surface using an infrared spectrometer (NICOLET iS10).

2.4. Phenanthrene adsorption

A stock solution of 1 g/L PHE in CH_2Cl_2 was prepared in advance. The concentrations of batch adsorption experiments ranged from 0.2 to 2 mg/L by diluting the stock solution with distilled water, followed by magnetic stirring to ensure the full dissolution (well-distributed at least) of PHE in water solutions. The adsorption was conducted in 100 mL brown conical flasks containing 30 mL PHE solution and 10 mg biochar. Duplicates and blanks were designed for all concentrations. All samples were put in a water bath shake in the dark at 25 ± 1℃ and shaken at 125 ± 5 rpm for 24 h to make sure of a full equilibrium of adsorption. After the equilibrium, the mixtures were filtered and the remaining PHE in the filtrate were enriched into 10 mL CH_2Cl_2 through solid-phase extraction, followed by concentration determination of PHE using

Shimadzu GCMS-QP2010 (please refer to Table S1 for details of method parameters). Afterward, a 2 mg/L PHE solution was used to investigate adsorption kinetics. Under the same experimental conditions described above, the mixtures were shaken at different durations from the beginning of the adsorption to up to 120 min. The residual PHE concentrations after each adsorption duration were measured by the same method as above.

The quantity of PHE adsorbed on the biochars is calculated using Eq. 1:

$$Q = (C_0 - C_e)V/M \quad (1)$$

where Q (μg/g) is the adsorption quantity, C_0 and C_e (μg/L) are the initial and equilibrium concentrations of PHE in water solutions, V (L) is the volume of the PHE solution for the adsorption, and M (g) is the mass of biochars used.

2.5. Computational simulations and calculations

The micro process of PHE adsorption on the biochar was investigated by the spin polarized DFT calculations performed with the Dmol^3 package. GGA-PBE was selected for the exchange-correlation potentials. The double numeric plus polarization basis set was applied in the local atomic orbital basis set with the global orbital cutoff 4.4 Å. Nudged elastic band tools of the Dmol^3 module and linear synchronous transit/quadratic synchronous transit were used to determine the energy barrier and minimum energy path for diffusion.

The adsorption energy is defined as Eq. 2:

$$E_{ad} = E_{total} - E_{subs} - E_{mole} \quad (2)$$

where E_{total}, E_{subs}, and E_{mole} represent the energy of substrate with adsorbate, substrate, and free molecule, respectively. Although the characteristics derived from the limited-sized model may not accurately reflect the actual system because of the size and edge effects, they still have qualitative reliability in predicting local chemical properties (Wang et al., 2019).

3. Results and discussion

3.1. Characterization of biochars

3.1.1. Morphological properties of biochars

SEM micrographs of biochars and PA powder are shown in Fig. 1. The structure of the raw material is in the form of sheet or block, thickly piling up with an irregular shape, and a large amount of debris is presented on the surface. For HABC and HMBC, the fibrous structure of the material was melted after HTC treatment. The SEM shows carbon microspheres of different sizes generated on the surface of HTC

biochars, which makes significant contributions in increasing the surface area of the biochar and enhancing the adsorption ability (Falco et al., 2013; Gao et al., 2013; Román et al., 2013). Nevertheless, the carbon microspheres formed on HABC have a smooth surface, excellent spherical shape, and superior dispersibility. In comparison, carbon microspheres formed on HMBC are stuck together into large pieces on the biochar surface, instead of being kept spherical. The phenomenon is due to the presence of additional gases released from the ammoniation reagent during the hydrothermal process, which slows down the polymerization of micronucleus of carbon microspheres on HABC surface and keeps them spherical. The pyrolyzed biochar, as shown in Fig. 1c, retains the fibrous structure of the raw material and just obtains a looser structure and rougher surface compared with the raw material.

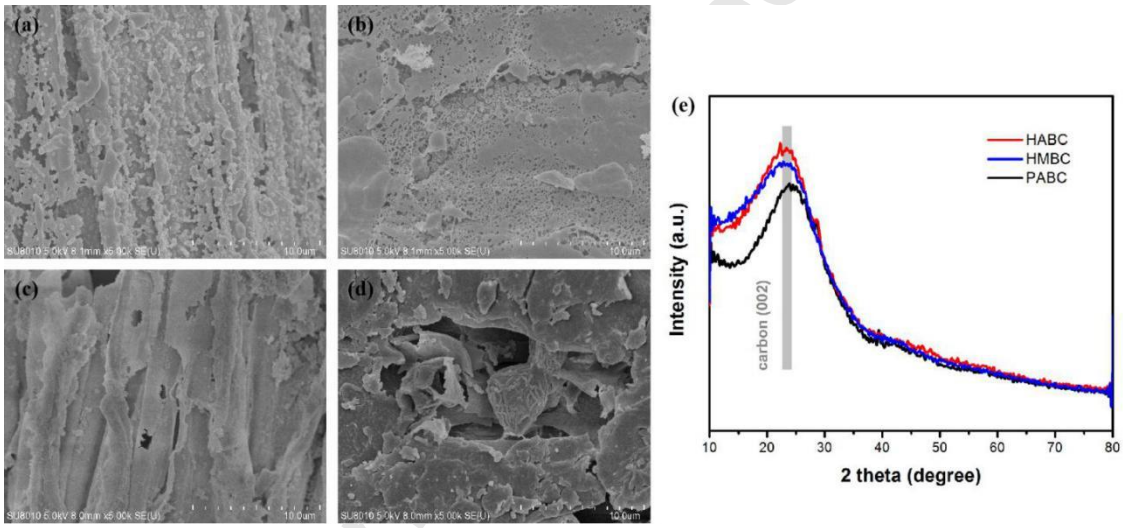

Fig. 1. SEM micrographs of biochars and PA powder, for (a) HABC, (b) HMBC, (c) PABC, and (d) PA powder. XRD patterns of biochars (e).

Figure 1e displays the XRD patterns of biochars. The broad peak occurs at around $2\theta = 23.5°$ in all samples could be assigned to the (002) plane of the crystal structure of graphitic carbon, which is somewhat incomplete and disordered (Yang et al., 2019). The diffracted intensities of HABC and HMBC are stronger than that of PABC, implying that the crystallinity of hydrothermal biochars is higher. This is possibly due to the hydrolysis of lignocellulose during the hydrothermal process, which made the side chains of cellulose disappear, followed by re-polymerization of aromatic compounds to form microcrystal structure (Lu et al., 2002; Hu et al., 2014). Since various crystal planes with different atomic arrangement and surface energy could lead to different binding energy with the adsorbate, the HTC biochars with higher crystallinity are deemed to have more (002) crystal planes with strong

adsorptivity, which is conducive to their adsorption ability.

3.1.2. Physical properties of biochars

Although biochar ordinarily has a relatively low specific surface area and porosity without further physical or chemical activation (Liu et al., 2015; Ding et al., 2019), the structural parameters exhibit apparent differences among the samples (Table S2). The HABC possessed the highest BET specific surface area of 22.385 m^2/g, owing to formation of a large number of dispersible carbon microspheres during hydrothermal process. Figure 2 shows the N_2 adsorption/desorption isotherms and pore size distributions of biochars. The isotherms are concave, with no knee points or saturated adsorption platforms. The concave is because of the stronger interaction within the adsorbed gas than that within the adsorbents. Accordingly, the adsorption process is difficult at the initial stage; however, with the increase of the relative pressure, the adsorption goes on and appears to be auto accelerated, and the number of adsorption layers is not limited (Sing, 1985). The adsorption amount of HABC is the highest, especially at high relative pressure, which was owing to surface adsorption to its largest outer surface. As shown in Fig. 2b, the higher porosity of HABC also facilitates the adsorption, possibly as a result of the joint effect of ammoniation reagent and water during hydrothermal treatment, which loosened the lignocellulose structure.

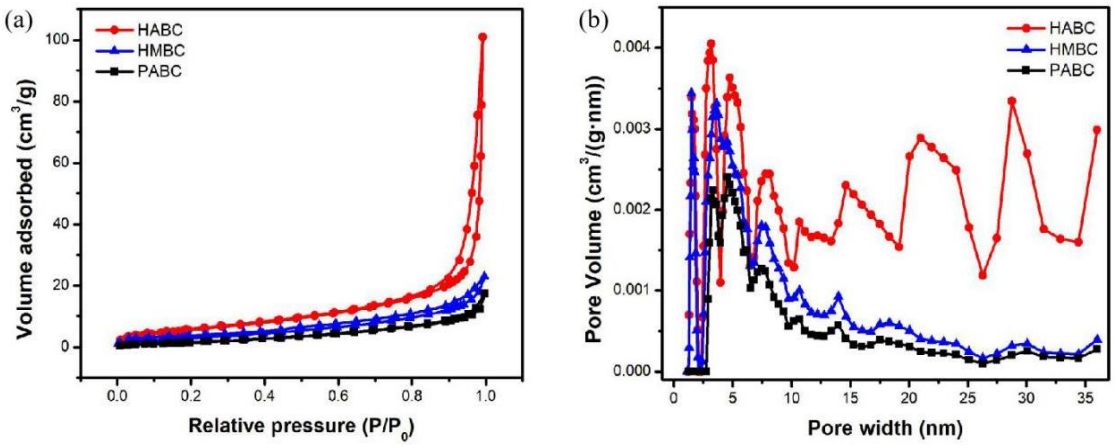

Fig. 2. N_2 adsorption/desorption isotherms (a) and pore size distributions (b) of biochars.

3.1.3. Chemical properties of biochars

The elemental composition of biochars is listed in Table 1. The pyrolysis of the raw material is characterized by decomposition and charring of lignocellulose, including several chemical reactions such as depolymerization, intramolecular rearrangement, decarboxylation, and dehydration (Shen et al., 2011). Part of the C

composition was converted into bio-oil and syngas (CO, CH_4, C_2H_2, etc.) (Liu et al., 2015), leading to a decline in C content in the final biochar product compared with the hydrothermal biochars. Decarboxylation and dehydration of hydrolysis products during HTC process released CO_2 and H_2O, causing the decrease of O content in HTC biochars (Sevilla and Fuertes, 2009). On average, HTC biochars exhibit higher C and lower O contents compared to pyrolyzed biochar. The O and C contents in HABC are reduced compared with HMBC, implying that O-containing functional groups were partially replaced by N functionalities; meanwhile, the C atoms were preferentially substituted by N atoms incorporated as graphitic N (Ding et al., 2019) or pyridine N (Gao et al., 2015), which is further proved by the deconvoluted N 1s XPS spectra of HABC. The N contents in HABC (5.48%) and PABC (1.22%) are much higher than that in HMBC (only 0.83%), indicating that the additive of ammoniation reagent made the biochar surface successfully doped with N.

Table 1

Elemental composition of biochar samples.

Samples	Relative content (%)				
	C	O	N	H	N/C
HABC	67.79	12.56	5.48	4.97	0.08
HMBC	72.87	17.60	0.83	4.79	0.01
PABC	56.47	22.51	1.22	2.64	0.02

FT-IR of the biochars before adsorption experiments are shown in Fig. 3a. The peak at around 3600 cm^{-1} may be attributed to the vibration of -OH stretching in alcohol (Huang et al., 2017). The peak at approximately 2920 cm^{-1} is due to the aliphatic C-H stretching model (Wang et al., 2019), which appears only in the HTC biochars, indicating the fracture of chemical bonds and hydrogenation during the hydrothermal treatment. Some intense bands near 1600 cm^{-1} may reflect the C=O and C=C aromatic rings stretching vibration, implying that biochars possess a structure in which aromatic carbon compounds play a central role, which can provide π-electrons (Hossain et al., 2011). The peak at 1415 cm^{-1} corresponding to CH_3 and CH_2 groups disappears in PABC because of the decomposition of chain hydrocarbons during pyrolysis (Jin et al., 2016). The band centered at 470 cm^{-1} is assigned to the C-N-C stretching vibration (Ge et al., 2016b). The ammoniated biochars showed higher intensity on this band, implying the influence of N-doping. Figure 3b, c, and d show the differences in FT-IR spectra before and after PHE adsorption. A boost in absorption intensity between 3600-3200 cm^{-1} can be seen in both samples, which is

assigned to O-H stretching vibration of hydroxyl functional groups, especially in the case of intermolecular association containing hydrogen bonds, indicating that PHE molecules were successfully adsorbed onto the biochar surface. In particular, the intensity at this range enhanced the most in HABC, implying the best adsorption ability of HABC.

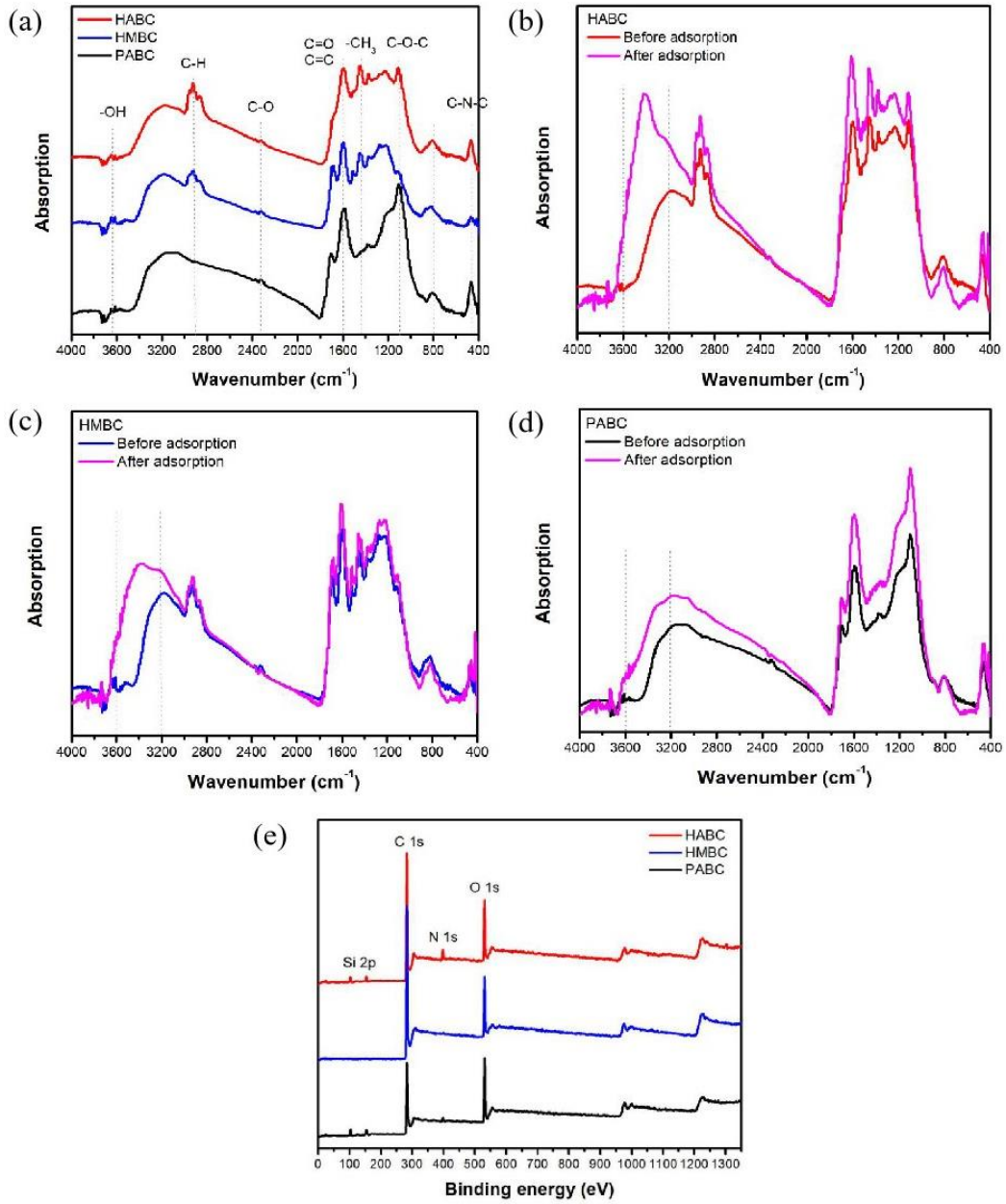

Fig. 3. FT-IR spectra of three biochars before PHE adsorption (a), FT-IR spectra before and after PHE adsorption (b, c, and d), and XPS survey spectra of three biochars (e).

The XPS survey spectra of biochars are shown in Fig. 3e. The peaks that reflect N 1s appeared in HABC and PABC, proving the successful doping of N in ammoniated biochars. The C 1s, O 1s, and N 1s spectra of three biochars and their deconvolutions are further analyzed in Fig. S1. C-C bonds in graphitic carbon take the

most significant proportion in HABC among three biochars, indicating a higher degree of graphitization in HABC. Other C forms are considered as C-O, C=O, and C-N (Valdés et al., 2002; Swiatkowski et al., 2004). The O 1s peaks are assigned to C=O in carbonyl or carboxyl groups, and C-OH or C-O-C in hydroxyl or ether groups (Martínez et al., 2003; Guo et al., 2017). In N 1s deconvolutions, the peaks representing -NH_2 exist in all samples. Notably, a peak located at 398.10 eV occurs in the HABC sample, which is assigned to pyridine N (Falco et al., 2013) and in agreement with the database (NIST XPS Database, Version 4.1). Besides, a small percentage of deconvolution is positioned at 401.11 eV, which represents graphitic N in HABC (Artyushkova et al., 2013). Both pyridine and graphitic N prove the substitution of C atoms by N after the ammoniation-hydrothermal treatment.

3.2. Phenanthrene adsorption experiments

3.2.1. Adsorption isotherms and kinetics

The adsorption isotherms are fitted with the Freundlich model. The equation is expressed in Eq. 3:

$$Q_e = K_F \cdot C_e^{\,n} \quad (3)$$

where Q_e (μg/g) is the adsorption quantity at equilibrium, K_F is the adsorption affinity parameter, C_e (μg/L) is the PHE concentration at equilibrium, and n is the nonlinear coefficient.

The isothermal curves of three biochars are shown in Fig. 4a and their K_F and n values for Freundlich model fitting equation are noted aside. The constants of Freundlich model and their values of R^2 are presented in Table S3. The fitting shows high values of R^2 (> 0.96), indicating that the Freundlich model can well explain the PHE adsorption on the biochars. Freundlich model is valid for heterogeneous surface, illustrating a complex physicochemical adsorption process, where the amount of PHE adsorbed on the biochar surface increases with the PHE concentration in solutions increasing (Vassileva et al., 2016). Values of n > 1 represent advantaged adsorption conditions (Rangabhashiyam et al., 2014), showing that the adsorption is inclined to carry out.

The adsorption kinetics are fitted with the Pseudo-first-order and Pseudo-second-order models. Equations are given in Eq. 4 and Eq. 5, respectively:

$$\ln(q_e - q_t) = \ln q_e - k_1 t \quad (4)$$

$$t/q_t = 1/k_2 q_e^{\,2} + t/q_e \quad (5)$$

where q_t (μg/g) is the adsorption quantity at a specific contact time t (min), q_e (μg/g)

is the adsorption quantity at equilibrium, k_1 (min^{-1}) is the rate constant of Pseudo-first-order model, and k_2 (g/(μg·min)) is the rate constant of Pseudo-second-order model.

The kinetic curves of three biochars are shown in Fig. 4b and their q_e values for Pseudo-second-order model fitting equation are noted aside. The parameters for Pseudo-first-order and Pseudo-second-order models and their values of R^2 are given in Table S3. PHE adsorption in this study is better fitted with Pseudo-second-order model with $R^2 > 0.82$ than Pseudo-first-order model ($R^2 < 0.76$), consistent with previous studies of PAHs adsorption (Zheng et al., 2018; Lamichhane et al., 2016; Ge et al., 2016a; Hu et al., 2014). The rate constant k_2 of HABC is 2.82 and 2.70 times of HMBC and PABC, respectively, showing that HABC has the best adsorption ability among the three. The maximum equilibrium adsorption capacity of HABC is 1.97 mg/g, much higher than that of several reported types of adsorbents such as coke activated carbon (Yuan et al., 2010) and modified bentonite (Changchaivong and Khaodhiar, 2009), and comparable to the adsorption capacity of fibrous membrane (Dai et al., 2013) (details are presented in Table S4).

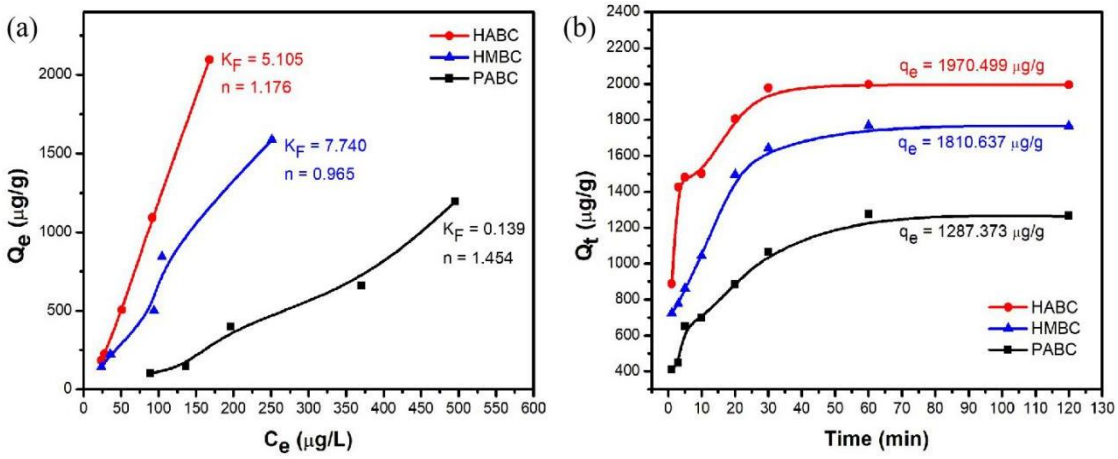

Fig. 4. PHE adsorption isotherms (a) and kinetics (b) onto three biochars.

3.2.2. Computational simulations and calculations based on DFT theory

The molecular models of PHE and biochar surface were constructed and optimized by BIOVIA Materials Studio, (Systèmes, 2017; Sharma et al., 2019a, 2019b). Details are shown in Fig. S2, S3, and Table S5, S6. The surface model of N-doped biochar is shown in Fig. 5a. As revealed in previous XPS analyses, the incorporated N atoms mainly exist in forms of graphitic N, pyridine N, and -NH_2 groups. The equilibrium configurations of PHE adsorption on active N functionalities are shown in Fig. 5b, c, d, and e, and the corresponding adsorption energy (binding

energy) is calculated based on DFT theory. The lower the adsorption energy, the more stable the adsorption system, and the stronger the binding ability. As listed in Table 2, the PHE binding ability of four configurations is in the following order: II > III > IV > I. The pyridine N shows the strongest binding ability, and the system is most stable when PHE binds with pyridine N in the form of configuration II.

PHE molecules have high π-electron density, and π-π interaction is most responsible for PHE adsorption except for the hydrophobic effect (Pei et al., 2013). In the N-doped HABC, the outer electrons of N atoms are sp^2-hybridized. In addition to bonding with the surrounding C atoms, they have lone pair electrons to form π-bonds with PHE molecules, acting as active adsorption sites where PHE molecules are preferentially adsorbed (Wang et al., 2014). Besides, the pyridine N increased the number of aromatic rings, which provides more π-electrons (Chen et al., 2018) and exhibits higher charge density. The electron cloud of PHE molecules overlapped with both lone pair electrons from N functionalities and π-electrons from aromatic structure, resulting in lower binding energy and stronger binding ability, therefore enhancing the adsorption ability. Moreover, in the case of graphitic N, the N atoms with stronger electronegativity than C atoms adjust the electronic structure of adjacent C and make their electrostatic potential distributions more positively charged (Ding et al., 2019). As revealed in Mulliken charge distributions (Fig. S4), the atomic charges of surrounding C atoms of graphitic N in HABC are 0.162 and 0.168, much higher than those in original biochar (-0.003, -0.001 and 0.001), making graphitic N a more electrophilic adsorption site and easier to bind with PHE molecules.

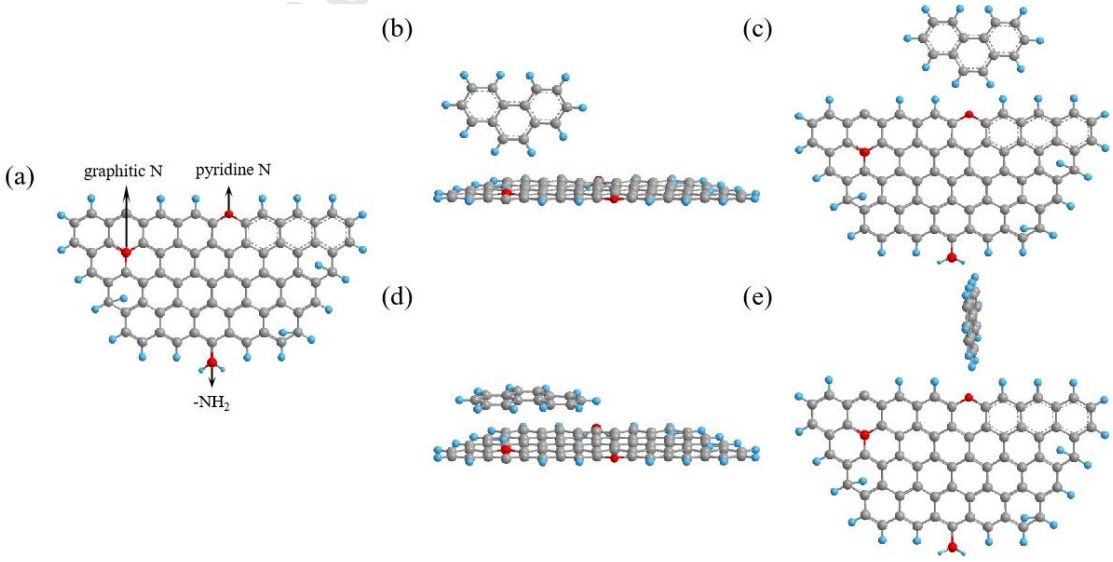

Fig. 5. Surface configurations of N-doped biochar (a) and different PHE adsorption configurations (I, II, III, and IV) on N-doped biochar surface (b, c, d, and e). Gray, blue, and red spheres represent C, H, and N atoms,

respectively.

Table 2

Adsorption energy of different PHE adsorption configurations on the N-doped biochar surface.

Adsorption configurations	Adsorption energy (eV)
I	-0.11
II	-0.43
III	-0.26
IV	-0.22

3.2.3. Stability and reusability of ammoniation-hydrothermal biochar

The stability and reusability of biochar are essential in practical application. To explore the stability of HABC after adsorption, XRD was applied to test its structural transformation (Li et al., 2019; Lai et al., 2019). The (002) peak shifts to a lower angle after adsorption in Fig. S5. According to Bragg's Law (Kacher et al., 2009), this could be caused by the existence of adsorbed PHE molecules, which extends the spacing of crystal planes in the graphitic structure. Also, a small peak appears at $2\theta = 42°$, implying the slight formation of (100/101) plane of graphitic structure. Such transformation has been reported by Kennedy et al. (2004) that due to the decomposition of carbon structures, some pores were created along the direction of graphitic structure. To further explore the reusability, saturated HABC was collected and regenerated by heating at 180℃ for 3 h (Qiao et al., 2018). The recovered HABC was used to run three cycle-experiments following the same steps in the previous kinetic experiment. As shown in Fig. S6, the maximum adsorption capacity decreases as the reuse time increases, 95.4%, 91.9%, and 87.3% of the initial adsorption quantity, respectively. The destruction of graphitic structure leads to degraded adsorption ability, partially caused by repeated high-temperature treatments (Salvador et al., 2015). However, the influence of regeneration temperature needs more in-depth investigations; besides, we will continue to optimize the HABC production to further enhance and ensure its stability.

4. Conclusions

Ammoniation-hydrothermal method was developed to prepare biochar with enhanced adsorption ability for PHE in aqueous solutions. The doped N functionalities, especially pyridine N, increased the aromatic structure and charge density of HABC, thus increasing the electron cloud overlapped degree between HABC and PHE molecules, resulting in lower binding energy and enhanced adsorption ability. The saturated HABC exhibited favorable reusability after three

cycles of regeneration. Further studies are required to improve the stability of HABC and regeneration method. The HABC could be used as an effective adsorbent for PHE adsorption from aqueous solutions.

Acknowledgments

This work was supported by the National Science Fund for Distinguished Young Scholars of China (No. 51925803), the National Natural Science Foundation of China (No. 51720105013 and 51878388), the Natural Science Foundation of Shandong Province (No. ZR2018QEE006), and Shandong Provincial Key Technology Research and Development Program (Major Scientific and Technological Innovation Project) (No. 2019JZZY010411).

Appendix A. Supporting information

Supplementary data associated with this article can be found in the online version.

References

Artyushkova, K., Kiefer, B., Halevi, B., Knop-Gericke, A., Schlogl, R., Atanassov, P., 2013. Density functional theory calculations of XPS binding energy shift for nitrogen-containing graphene-like structures. CHEM COMMUN 49, 2539-2541. https://doi.org/10.1039/c3cc40324f

Benavente, V., Calabuig, E., Fullana, A., 2015. Upgrading of moist agro-industrial wastes by hydrothermal carbonization. J ANAL APPL PYROL 113, 89-98. https://doi.org/10.1016/j.jaap.2014.11.004

Chang, B.V., Chang, S.W., Yuan, S.Y., 2003. Anaerobic degradation of polycyclic aromatic hydrocarbons in sludge. Advances in Environmental Research 7, 623-628. https://doi.org/10.1016/S1093-0191(02)00047-3

Changchaivong, S., Khaodhiar, S., 2009. Adsorption of naphthalene and phenanthrene on dodecylpyridinium-modified bentonite. APPL CLAY SCI 43, 317-321. https://doi.org/10.1016/j.clay.2008.09.012

Chen, Q., Zheng, J., Zheng, L., Dang, Z., Zhang, L., 2018. Classical theory and electron-scale view of exceptional Cd(II) adsorption onto mesoporous cellulose biochar via experimental analysis coupled with DFT calculations. CHEM ENG J, 1000-1009. https://doi.org/10.1016/j.cej.2018.06.054

Dai, Y., Niu, J., Yin, L., Xu, J., Xu, J., 2013. Laccase-carrying electrospun fibrous membrane for the removal of polycyclic aromatic hydrocarbons from contaminated water. SEP PURIF TECHNOL 104, 1-8. https://doi.org/10.1016/j.seppur.2012.11.013

Ding, D., Yang, S., Qian, X., Chen, L., Cai, T., 2019. Nitrogen-doping positively whilst sulfur-doping negatively affect the catalytic activity of biochar for the degradation of organic contaminant. Applied Catalysis B: Environmental, 118348. https://doi.org/10.1016/j.apcatb.2019.118348

Falco, C., Marco-Lozar, J.P., Salinas-Torres, D., Morallón, E., Cazorla-Amorós, D., Titirici, M.M., Lozano-Castelló, D., 2013. Tailoring the porosity of chemically activated hydrothermal carbons:

Influence of the precursor and hydrothermal carbonization temperature. CARBON 62, 346-355. https://doi.org/10.1016/j.carbon.2013.06.017

Gao, F., Shao, G., Qu, J., Lv, S., Li, Y., Wu, M., 2015. Tailoring of porous and nitrogen-rich carbons derived from hydrochar for high-performance supercapacitor electrodes. ELECTROCHIM ACTA 155, 201-208. https://doi.org/10.1016/j.electacta.2014.12.069

Gao, Y., Wang, X., Wang, J., Li, X., Cheng, J., Yang, H., Chen, H., 2013. Effect of residence time on chemical and structural properties of hydrochar obtained by hydrothermal carbonization of water hyacinth. ENERGY 58, 376-383. https://doi.org/10.1016/j.energy.2013.06.023

Ge, X., Wu, Z., Wu, Z., Yan, Y., Cravotto, G., Ye, B., 2016a. Enhanced PAHs adsorption using iron-modified coal-based activated carbon via microwave radiation. J TAIWAN INST CHEM E 64, 235-243. https://doi.org/10.1016/j.jtice.2016.03.050

Ge, X., Wu, Z., Wu, Z., Yan, Y., Cravotto, G., Ye, B., 2016b. Microwave-assisted modification of activated carbon with ammonia for efficient pyrene adsorption. J IND ENG CHEM 39, 27-36. https://doi.org/10.1016/j.jiec.2016.05.003

Givens, D.I., Adamson, A.H., Cobby, J.M., 1988. The effect of ammoniation on the nutritive value of wheat, barley and oat straws. II. Digestibility and energy value measurements in vivo and their prediction from laboratory measurements. ANIM FEED SCI TECH 19, 173-184. https://doi.org/10.1016/0377-8401(88)90065-X

Guo, Z., Zhang, A., Zhang, J., Liu, H., Kang, Y., Zhang, C., 2017. An ammoniation-activation method to prepare activated carbon with enhanced porosity and functionality. POWDER TECHNOL 309, 74-78. https://doi.org/10.1016/j.powtec.2016.12.068

Gupta, H., 2016. Photocatalytic degradation of phenanthrene in the presence of akaganeite nano-rods and the identification of degradation products. RSC ADV 6, 112721-112727. https://doi.org/10.1039/c6ra24602h

Gupta, H., Singh, S., 2018. Kinetics and thermodynamics of phenanthrene adsorption from water on orange rind activated carbon. Environmental Technology & Innovation 10, 208-214. https://doi.org/10.1016/j.eti.2018.03.001

Gupta, V.K., Nayak, A., Agarwal, S., Tyagi, I., 2014. Potential of activated carbon from waste rubber tire for the adsorption of phenolics: Effect of pre-treatment conditions. J COLLOID INTERF SCI 417, 420-430. https://doi.org/10.1016/j.jcis.2013.11.067

Hossain, M.K., Strezov, V., Chan, K.Y., Ziolkowski, A., Nelson, P.F., 2011. Influence of pyrolysis temperature on production and nutrient properties of wastewater sludge biochar. J ENVIRON MANAGE 92, 223-228. https://doi.org/10.1016/j.jenvman.2010.09.008

Hu, J., Shen, D., Wu, S., Zhang, H., Xiao, R., 2014. Effect of temperature on structure evolution in char from hydrothermal degradation of lignin. J ANAL APPL PYROL 106, 118-124. https://doi.org/10.1016/j.jaap.2014.01.008

Huang, H., Yang, T., Lai, F., Wu, G., 2017. Co-pyrolysis of sewage sludge and sawdust/rice straw for the production of biochar. J ANAL APPL PYROL 125, 61-68. https://doi.org/10.1016/j.jaap.2017.04.018

Huang, Q., Song, S., Chen, Z., Hu, B., Chen, J., Wang, X., 2019. Biochar-based materials and their applications in removal of organic contaminants from wastewater: State-of-the-art review. Biochar 1, 45-73. https://doi.org/10.1007/s42773-019-00006-5

Jin, J., Li, Y., Zhang, J., Wu, S., Cao, Y., Liang, P., Zhang, J., Wong, M.H., Wang, M., Shan, S., Christie, P., 2016. Influence of pyrolysis temperature on properties and environmental safety of heavy metals in biochars derived from municipal sewage sludge. J HAZARD MATER 320, 417-426. https://doi.org/10.1016/j.jhazmat.2016.08.050

Kacher, J., Landon, C., Adams, B.L., Fullwood, D., 2009. Bragg's Law diffraction simulations for electron backscatter diffraction analysis. ULTRAMICROSCOPY 109, 1148-1156. https://doi.org/10.1021/ie034093f

Kaya, E.M.Ö., Özcan, A.S., Gök, Ö., Özcan, A., 2013. Adsorption kinetics and isotherm parameters of naphthalene onto natural and chemically modified bentonite from aqueous solutions. ADSORPTION 19, 879-888. https://doi.org/10.1007/s10450-013-9542-3

Kennedy, L.J., Vijaya, J.J., Sekaran, G., 2004. Effect of Two-Stage Process on the Preparation and Characterization of Porous Carbon Composite from Rice Husk by Phosphoric Acid Activation. IND ENG CHEM RES 43, 1832-1838. https://doi.org/10.1021/ie034093f

Khan, A., Wang, J., Li, J., Wang, X., Chen, Z., Alsaedi, A., Hayat, T., Chen, Y., Wang, X., 2017. The role of graphene oxide and graphene oxide-based nanomaterials in the removal of pharmaceuticals from aqueous media: A review. ENVIRON SCI POLLUT R 24, 7938-7958. https://doi.org/10.1007/s11356-017-8388-8

Lai, C., Huang, F., Zeng, G., Huang, D., Qin, L., Cheng, M., Zhang, C., Li, B., Yi, H., Liu, S., Li, L., Chen, L., 2019. Fabrication of novel magnetic MnFe2O4/bio-char composite and heterogeneous photo-Fenton degradation of tetracycline in near neutral pH. CHEMOSPHERE 224, 910-921. https://doi.org/10.1016/j.chemosphere.2019.02.193

Lamichhane, S., Bal Krishna, K.C., Sarukkalige, R., 2016. Polycyclic aromatic hydrocarbons (PAHs) removal by sorption: A review. CHEMOSPHERE 148, 336-353. https://doi.org/10.1016/j.chemosphere.2016.01.036

Lee, S., Park, S., 2013. TiO_2 photocatalyst for water treatment applications. J IND ENG CHEM 19, 1761-1769. https://doi.org/10.1016/j.jiec.2013.07.012

Li, L., Lai, C., Huang, F., Cheng, M., Zeng, G., Huang, D., Li, B., Liu, S., Zhang, M., Qin, L., Li, M., He, J., Zhang, Y., Chen, L., 2019. Degradation of naphthalene with magnetic bio-char activate hydrogen peroxide: Synergism of bio-char and Fe-Mn binary oxides. WATER RES 160, 238-248. https://doi.org/10.1016/j.watres.2019.05.081

Liu, W., Jiang, H., Yu, H., 2015. Development of Biochar-Based Functional Materials: Toward a Sustainable Platform Carbon Material. CHEM REV 115, 12251-12285. https://doi.org/10.1021/acs.chemrev.5b00195

Lu, L., Kong, C., Sahajwalla, V., Harris, D., 2002. Char structural ordering during pyrolysis and combustion and its influence on char reactivity. FUEL 81, 1215-1225. https://doi.org/10.1016/S0016-2361(02)00035-2

Martínez, M.T., Callejas, M.A., Benito, A.M., Cochet, M., Seeger, T., Ansón, A., Schreiber, J., Gordon, C., Marhic, C., Chauvet, O., Fierro, J.L.G., Maser, W.K., 2003. Sensitivity of single wall carbon nanotubes to oxidative processing: Structural modification, intercalation and functionalisation. CARBON 41, 2247-2256. https://doi.org/10.1016/S0008-6223(03)00250-1

Mittal, A., Thakur, V., Gajbe, V., 2013. Adsorptive removal of toxic azo dye Amido Black 10B by hen feather. ENVIRON SCI POLLUT R 20, 260-269. https://doi.org/10.1007/s11356-012-0843-y

Moon, S., Shim, J., 2006. A novel process for CO_2/CH_4 gas separation on activated carbon fibers-electric swing adsorption. J COLLOID INTERF SCI 298, 523-528. https://doi.org/10.1016/j.jcis.2005.12.052

Mumme, J., Eckervogt, L., Pielert, J., Diakité, M., Rupp, F., Kern, J., 2011. Hydrothermal carbonization of anaerobically digested maize silage. BIORESOURCE TECHNOL 102, 9255-9260. https://doi.org/10.1016/j.biortech.2011.06.099

NIST X-ray Photoelectron Spectroscopy Database, NIST Standard Reference Database Number 20, National Institute of Standards and Technology, Gaithersburg MD, 20899 (2000). http://dx.doi.org/10.18434/T4T88K

Pang, H., Wu, Y., Wang, X., Hu, B., Wang, X., 2019. Recent Advances in Composites of Graphene and Layered Double Hydroxides for Water Remediation: A Review. Chemistry - An Asian Journal 14, 2542-2552. https://doi.org/10.1002/asia.201900493

Pei, Z., Li, L., Sun, L., Zhang, S., Shao, X., Yang, S., Wen, B., 2013. Adsorption characteristics of 1,2,4-trichlorobenzene, 2,4,6-trichlorophenol, 2-naphthol and naphthalene on graphene and graphene oxide. CARBON 51, 156-163. https://doi.org/10.1016/j.carbon.2012.08.024

Qiao, K., Tian, W., Bai, J., Dong, J., Zhao, J., Gong, X., Liu, S., 2018. Preparation of biochar from *Enteromorpha prolifera* and its use for the removal of polycyclic aromatic hydrocarbons (PAHs) from aqueous solution. ECOTOX ENVIRON SAFE 149, 80-87. https://doi.org/10.1016/j.ecoenv.2017.11.027

Rangabhashiyam, S., Anu, N., Giri Nandagopal, M.S., Selvaraju, N., 2014. Relevance of isotherm models in biosorption of pollutants by agricultural byproducts. Journal of Environmental Chemical Engineering 2, 398-414. https://doi.org/10.1016/j.jece.2014.01.014

Reza, M.T., Andert, J., Wirth, B., Busch, D., Pielert, J., Lynam, J.G., Mumme, J., 2014. Hydrothermal carbonization of biomass for energy and crop production. APPLIED BIOENERGY 1, 11-29. https://doi.org/10.2478/apbi-2014-0001

Salvador, F., Martin-Sanchez, N., Sanchez-Hernandez, R., Sanchez-Montero, M.J., Izquierdo, C., 2015. Regeneration of carbonaceous adsorbents. Part I: Thermal Regeneration. MICROPOR MESOPOR MAT 202, 259-276. https://doi.org/10.1016/j.micromeso.2014.02.045

Sevilla, M., Fuertes, A.B., 2009. The production of carbon materials by hydrothermal carbonization of cellulose. CARBON 47, 2281-2289. https://doi.org/10.1016/j.carbon.2009.04.026

Sharma, S., Kumar, P., Chandra, R., 2019a. Applications of BIOVIA Materials Studio, LAMMPS, and GROMACS in Various Fields of Science and Engineering. In: Sharma, S. (Ed.). Molecular Dynamics Simulation of Nanocomposites Using BIOVIA Materials Studio, Lammps and Gromacs. Elsevier, pp. 329-341. https://doi.org/10.1016/B978-0-12-816954-4.00007-3

Sharma, S., Kumar, P., Chandra, R., 2019b. Overview of BIOVIA Materials Studio, LAMMPS, and GROMACS. In: Sharma, S. (Ed.). Molecular Dynamics Simulation of Nanocomposites Using BIOVIA Materials Studio, Lammps and Gromacs. Elsevier, pp. 39-100. https://doi.org/10.1016/B978-0-12-816954-4.00002-4

Shen, D., Xiao, R., Gu, S., Luo, K., 2011. The pyrolytic behavior of cellulose in lignocellulosic biomass: A review. RSC ADV 1, 1641-1660. https://doi.org/10.1039/c1ra00534k

Sing, K.S., 1985. Reporting Physisorption Data for Gas/Solid Systems with Special Reference to the Determination of Surface Area and Porosity. PURE APPL CHEM 57, 603-619. http://dx.doi.org/10.1351/pac198557040603

Swiatkowski, A., Pakula, M., Biniak, S., Walczyk, M., 2004. Influence of the surface chemistry of modified activated carbon on its electrochemical behaviour in the presence of lead(II) ions. CARBON 42, 3057-3069. https://doi.org/10.1016/j.carbon.2004.06.043

Systèmes, D., 2017. Dassault Systèmes BIOVIA, materials studio., San Diego.

Valdés, H., Sánchez-Polo, M., Rivera-Utrilla, J., Zaror, C.A., 2002. Effect of ozone treatment on surface properties of activated carbon. LANGMUIR 18, 2111-2116. https://doi.org/10.1021/la010920a

Vassileva, P.S., Radoykova, T.H., Detcheva, A.K., Avramova, I.A., Aleksieva, K.I., Nenkova, S.K., Valchev, I.V., Mehandjiev, D.R., 2016. Adsorption of Ag^{+} ions on hydrolyzed lignocellulosic materials based on willow, paulownia, wheat straw and maize stalks. INT J ENVIRON SCI TE 13, 1319-1328. https://doi.org/10.1007/s13762-016-0970-y

Wang, H., Guo, W., Liu, B., Wu, Q., Luo, H., Zhao, Q., Si, Q., Sseguya, F., Ren, N., 2019. Edge-nitrogenated biochar for efficient peroxydisulfate activation: An electron transfer mechanism. WATER RES 160, 405-414. https://doi.org/10.1016/j.watres.2019.05.059

Wang, J., Chen, Z., Chen, B., 2014. Adsorption of polycyclic aromatic hydrocarbons by graphene and graphene oxide nanosheets. ENVIRON SCI TECHNOL 48, 4817-4825. https://doi.org/10.1021/es405227u

Wang, X., Chi, Q., Liu, X., Wang, Y., 2019. Influence of pyrolysis temperature on characteristics and environmental risk of heavy metals in pyrolyzed biochar made from hydrothermally treated sewage sludge. CHEMOSPHERE 216, 698-706. https://doi.org/10.1016/j.chemosphere.2018.10.189

Wang, Y., Li, Y., Zhang, Y., Wei, W., 2019. Effects of macromolecular humic/fulvic acid on Cd(II) adsorption onto reed-derived biochar as compared with tannic acid. INT J BIOL MACROMOL 134, 43-55. https://doi.org/10.1016/j.ijbiomac.2019.05.039

Wang, Y., Zhang, Y., Li, S., Zhong, W., Wei, W., 2018. Enhanced methylene blue adsorption onto activated reed-derived biochar by tannic acid. J MOL LIQ 268, 658-666. https://doi.org/10.1016/j.molliq.2018.07.085

Yakout, S.M., Daifullah, A.A.M., El-Reefy, S.A., 2013. Adsorption of Naphthalene, Phenanthrene and Pyrene from Aqueous Solution Using Low-Cost Activated Carbon Derived from Agricultural Wastes. ADSORPT SCI TECHNOL 31, 293-302. https://doi.org/10.1260/0263-6174.31.4.293

Yang, Z., Chen, B., Chen, W., Qu, Y., Zhou, F., Zhao, C., Xu, Q., Zhang, Q., Duan, X., Wu, Y., 2019. Directly transforming copper (I) oxide bulk into isolated single-atom copper sites catalyst through gas-transport approach. NAT COMMUN 10, 3734. https://doi.org/10.1038/s41467-019-11796-4

Yuan, M., Tong, S., Zhao, S., Jiac, C.Q., 2010. Adsorption of polycyclic aromatic hydrocarbons from water using petroleum coke-derived porous carbon. J HAZARD MATER 181, 1115-1120. https://doi.org/10.1016/j.jhazmat.2010.05.130

Zhang, H., Wang, Z., Li, R., Guo, J., Li, Y., Zhu, J., Xie, X., 2017. TiO_2 supported on reed straw biochar as an adsorptive and photocatalytic composite for the efficient degradation of

sulfamethoxazole in aqueous matrices. CHEMOSPHERE 185, 351-360. https://doi.org/10.1016/j.chemosphere.2017.07.025

Zhang, Z., Zhu, Z., Shen, B., Liu, L., 2019. Insights into biochar and hydrochar production and applications: A review. ENERGY 171, 581-598. https://doi.org/10.1016/j.energy.2019.01.035

Zheng, X., Lin, H., Tao, Y., Zhang, H., 2018. Selective adsorption of phenanthrene dissolved in Tween 80 solution using activated carbon derived from walnut shells. CHEMOSPHERE 208, 951-959. https://doi.org/10.1016/j.chemosphere.2018.06.025